

Considerations in Modelling the Melting of Fuel Containing Fission Products and Solute Oxides

F. Akbari, M.J. Welland, B.J. Lewis and W.T. Thompson

*Department of Chemistry and Chemical Engineering, Royal Military College of Canada,
Kingston, Ontario K7K 7B4*

ABSTRACT

It is well known that the oxidation of a defected fuel element by steam gives rise to an increase in O/U ratio with a consequent lowering of the incipient melting temperature. Concurrently, the hyperstoichiometry reduces the thermal conductivity thereby raising the centerline fuel pellet temperature for a fixed linear power. The development of fission products soluble in the UO_2 phase or, more important, the deliberate introduction of additive oxides in advanced CANDU fuel bundle designs further affects and generally lowers the incipient melting temperature. For these reasons, the modeling of the molten (hyperstoichiometric) UO_2 phase containing several solute oxides (ZrO_2 , Ln_2O_3 and AnO_2) is advancing in the expectation of developing a moving boundary heat and mass transfer model aimed at better defining the limits of safe operating practice as burnup advances.

The paper describes how the molten phase stability model is constructed. The redistribution of components across the solid-liquid interface that attends the onset of melting of a non-stoichiometric UO_2 containing several solutes will be discussed. The issues of how to introduce boundary conditions into heat transfer calculations consistent with the requirements of the Phase Rule will be addressed. The Stefan problem of a moving boundary associated with the solid/liquid interface sets this treatment apart from conventional heat and mass transfer problems.

1.0 THERMODYNAMIC CONSIDERATIONS

(i) U-O System (near melting point and effect of pressure)

A thermodynamic treatment for the U-O binary system, the cornerstone of any fuel model, was previously developed by the authors placing emphasis on the solid phases, and in particular, the non stoichiometry of the UO_{2+x} phase⁽¹⁾. Figure 1 shows the detail near the melting of UO_{2+x} . The features are consistent with recent evaluations by Chevalier *et. al.*⁽²⁾ and Guéneau *et. al.*⁽³⁾. The composition in Figure 1 is expressed in terms of the formal components UO_2 and UO_3 where it is to be noted that the mole fraction of UO_3 (X_{UO_3}) is numerically the same as x in the subscript of the formulation UO_{2+x} (i.e., $x = X_{\text{UO}_3}$). The recent measurements for solidus and liquidus temperatures by Manara *et. al.*⁽⁵⁾ are placed on Figure 1. In view of the extremely high temperature, it is understandable that there is still uncertainty in the exact placement of the phase boundaries but the topology is generally agreed upon.

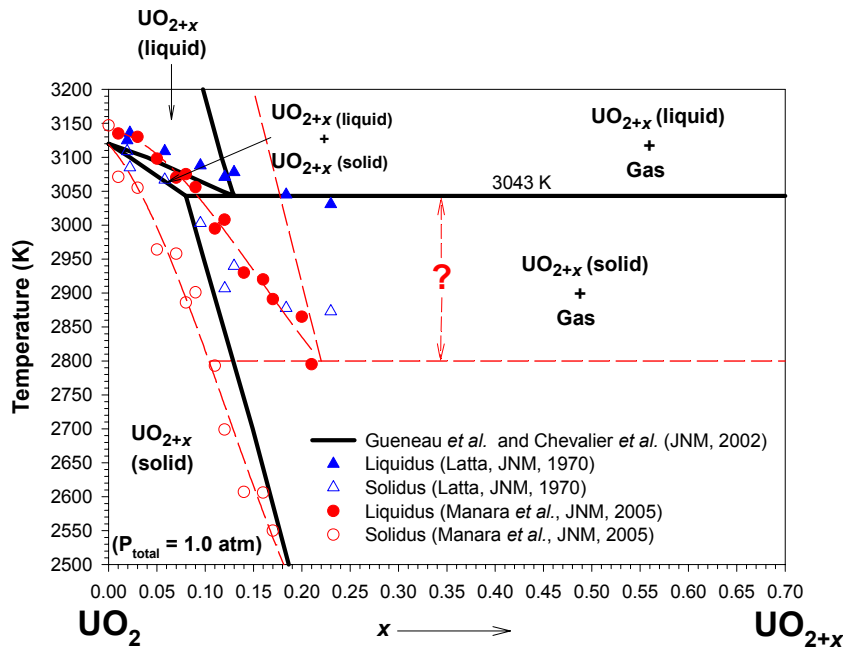
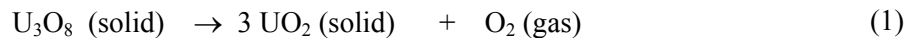


Figure 1: Solidus and liquidus associated with the melting of UO_{2+x} . The gas phase field boundaries apply to 1.0 atm (absolute) total pressure. The question mark and broken line pertain to the 250 K uncertainty in the lower temperature where molten hyperstoichiometric oxide may possibly exist (at 1.0 atm).

An important feature in Figure 1 is the presence of a gas phase at high levels of hyperstoichiometry. The gas phase in this diagram is not pure oxygen (at 1 atm (absolute) pressure) but instead contains a concentration of UO_3 vapour that increases with temperature. Although the hydrostatic pressure applicable to most phase diagrams is generally understood to be 1 atm unless specified otherwise, the pressure of coolant in the CANDU reactor is approximately 100 atm. Therefore, the effect of pressure on the phase diagram is important. For equilibrium among condensed phases, the influence is small for such a pressure increase. However, the influence is significant in relation to the phase boundaries bordering the gas phase. The effect is shown in Figure 2. It can be seen that the enhancement of pressure increases the solubility of oxygen in both the UO_{2+x} solid and liquid phases. This effect prolongs downward the solidus and liquidus lines extending from pure UO_2 . The reaction representing the dissociation of U_3O_8 , is also affected by pressure:



At a higher oxygen (partial) pressure, U_3O_8 decomposes at a higher temperature. At a calculated total pressure of 56.4 atm, solid UO_{2+x} and U_3O_8 may come into equilibrium with molten oxide. The minimum temperature at which liquid oxide can be expected is thus not 3043K (solid lines in Figure 1) but rather 2743K for pressures greater than 56.4 atm. Liquid oxide may exist at a temperature 300K lower than expected if the UO_{2+x} is sufficiently hyperstoichiometric.

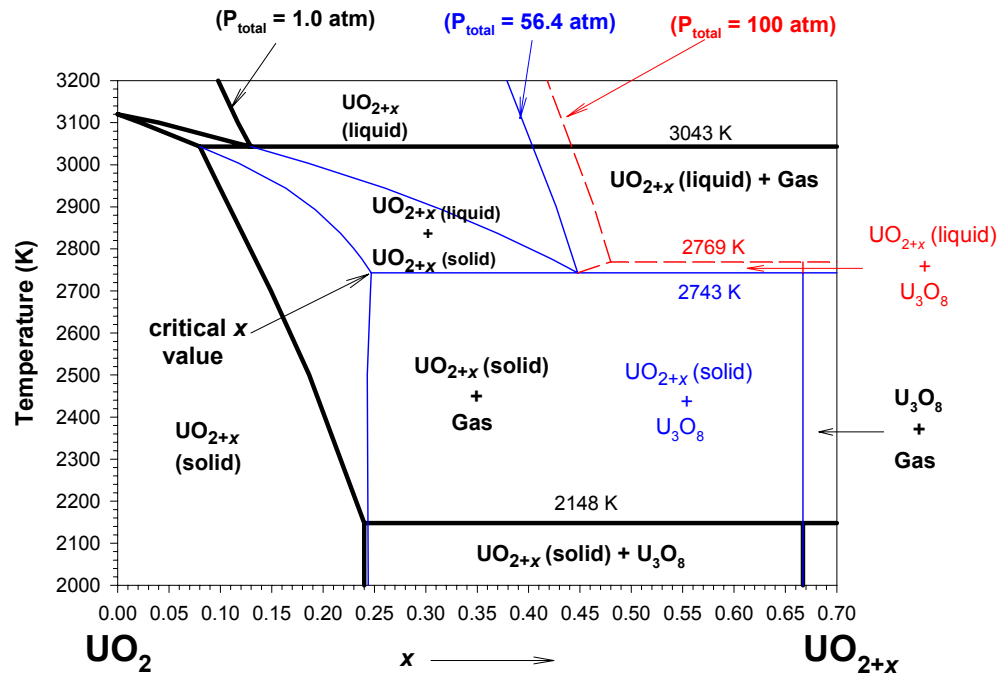
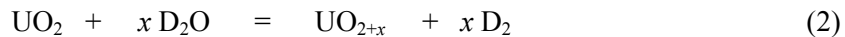


Figure 2: Effect of total pressure on the phase diagram of U-O system. Increasing the total pressure above 56.4 atm lowers the temperature where liquid oxide can exist by 300 K.

The question now arises about how the stoichiometry of the UO_{2+x} phase can be increased to the critical value associated with the left end of the eutectic tie line at 2743K in Figure 2. In a situation of practical interest coolant heavy water vapour can react with fuel at a sheathing breach. As the fuel is oxidized deuterium gas is produced:



The driving force for the continued oxidation or shift of the reaction (2) to the right, is the D_2O partial pressure. The driving force for the reverse reaction increases as the D_2 partial pressure builds. Since both gases in equation (2) are preceded by the same mole number (x), the shift in stoichiometry of the UO_2 expressed by the value of x is proportional to the ratio of the D_2O and D_2 partial pressures.

Thus, it is useful to place lines of constant $\text{H}_2\text{O}/\text{H}_2$ ($\text{D}_2\text{O}/\text{D}_2$) ratio that create in effect the oxygen partial pressure associated with a particular degree of hyperstoichiometry. These lines are depicted on Figure 3. Of course, increasing the O/U ratio of the UO_{2+x} fuel is accompanied by an increase in the partial pressure of UO_3 vapour, so these isobars also appear on Figure 3. As a comparison of the O_2 and UO_3 isobars in Figure 3 makes clear, O_2 is the main component in the gas phase at the lower temperatures near the bottom of the figure. At higher temperatures, evaporation of UO_3 becomes progressively more important. Furthermore, oxygen itself will dissociate into atomic oxygen to some degree. Figure 4 shows the sum of the partial pressures, $p_{\text{UO}_2} + p_{\text{UO}_3} + p_{\text{O}}$, over molten stoichiometric UO_2 computed in the present work in comparison

with those proposed by Fink⁽⁶⁾. There is reasonable agreement near the melting temperature of UO_2 although the projections to extremely high temperature diverge. It is apparent that pressure has a strong effect on the phase equilibrium in the U-O system, a matter, which is complicated by the co-existence of five or more significant vapour species (H_2O , H_2 , UO_2 , UO_3 , O_2 , O).

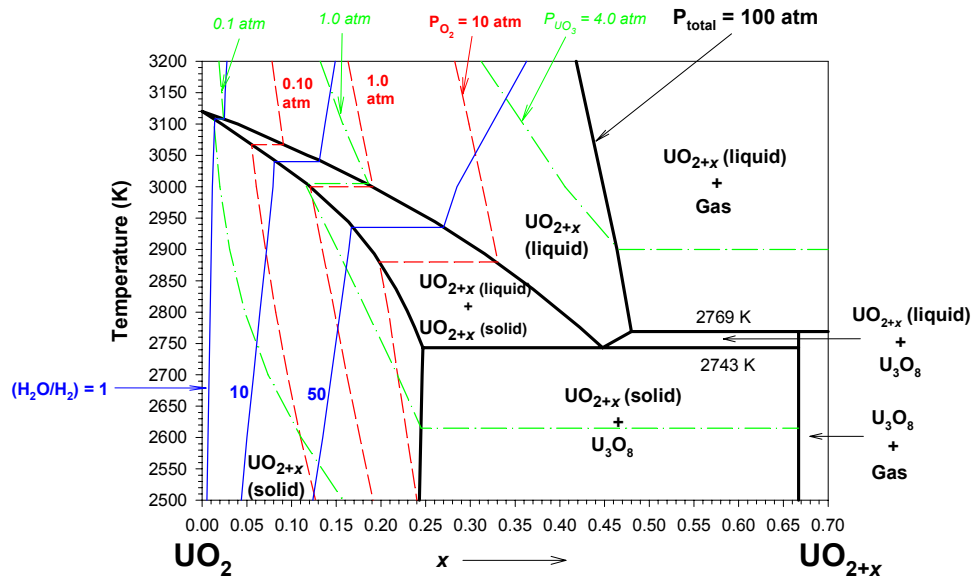


Figure 3: Influence of O_2 and UO_3 partial pressure as well as $(\text{H}_2\text{O}/\text{H}_2)$ ratio on phase equilibrium in the U-O system at high pressure.

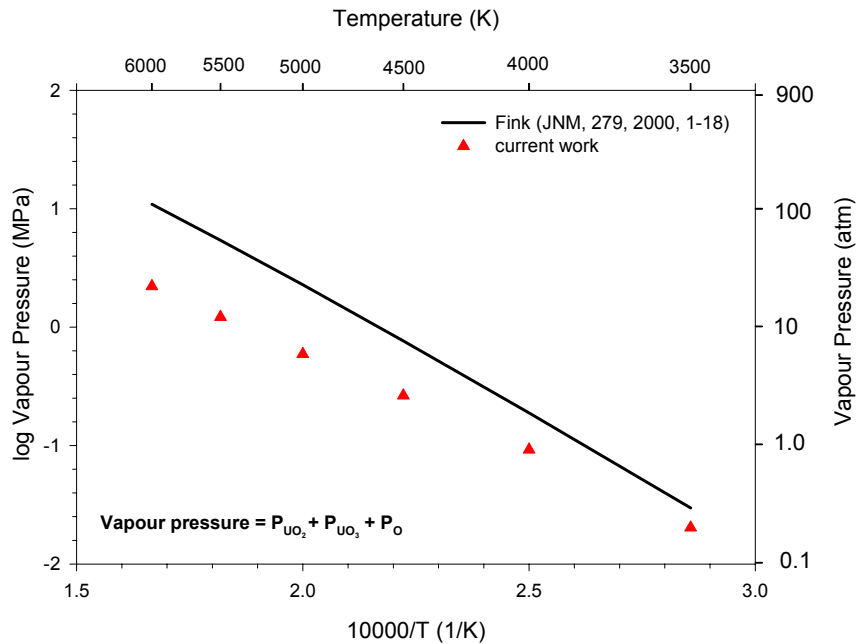


Figure 4: Total pressure ($p_{\text{UO}_2} + p_{\text{UO}_3} + p_{\text{O}}$) over molten stoichiometric UO_2 at high temperatures. The treatments concur near the melting point.

(ii) *Enthalpy changes*

An essential thermodynamic property in heat transfer modelling is the enthalpy. Enthalpy change is calculated by integrating heat capacity over the desired temperature span. The heat capacity and related enthalpy change over the temperature range of 2500-3500 K is shown for UO_2 and $\text{UO}_{2.05}$ solid and liquid phases in Figure 5. The data for UO_2 was taken from Fink⁽⁶⁾; for $\text{UO}_{2.05}$ the development is based on a previous publication by authors⁽¹⁾. Since, UO_2 is a stoichiometric phase, it melts at constant temperature (3120 K), the enthalpy of melting at this temperature is 70 kJ mol^{-1} . However, $\text{UO}_{2.05}$ melts over a calculated 22 degree temperature range (3072-3094 K) and the calculated enthalpy of melting is slightly higher than that for pure UO_2 . It is noticeable that the heat capacity of liquid UO_2 is lower than solid UO_2 . Great significance should not be attributed to the difference in the temperature dependence of the heat capacity of liquid as it increases in O/U ratio. There is little data available to settle this matter.

Near 2670 K there is a second order, “ λ transition”, or phase transformation in solid UO_2 . Matweev and Veshchunov⁽⁷⁾ recently suggested a microscopic model for superionic transition of UO_2 at temperatures around 2670 K. They have used this model to explain a spike in the heat capacity of uranium oxide otherwise called a Bredig transition. Such a spike calls for measurements of enthalpy change *in addition to the heat capacity* since it is impractical to evaluate the step in enthalpy in passing through such a transformation by the integration of the (approximate) heat capacity across the temperature range (thought to be about 80 K) over which it occurs.

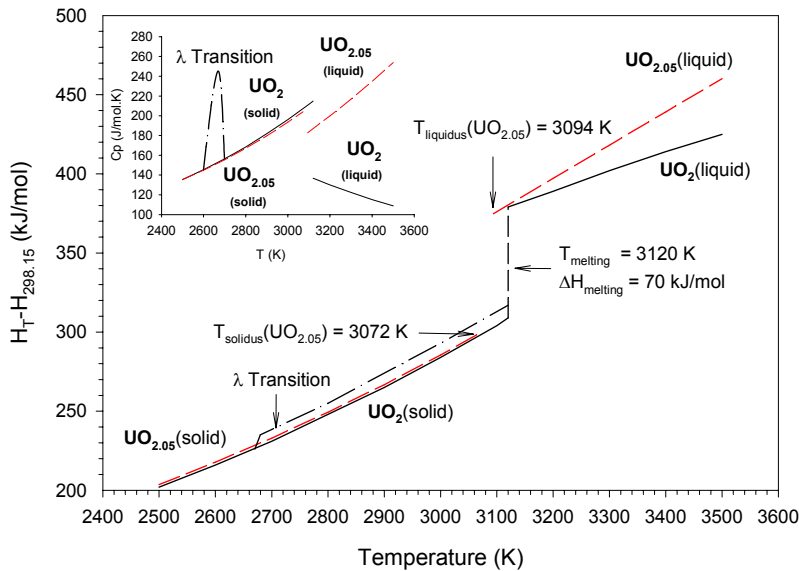


Figure 5: Enthalpy (kJ mol^{-1}) and specific heat capacity ($\text{J mol}^{-1} \text{K}^{-1}$) changes with temperature for UO_2 and $\text{UO}_{2.05}$ solid and liquid phases. Significance of the spike in heat capacity near 2670 K on the enthalpy of UO_2 solid.

Although it is conventional to display binary phase diagrams on temperature-composition co-ordinates, it is useful for the intended application to replace temperature with the equivalent

enthalpy change. The ability to do this is one of the benefits that accompanies phase diagram development by modelling the underlying thermodynamic properties. Figure 6 shows the U-O system on these co-ordinates near the melting of UO_2 . The enthalpy change for melting can be compared with the steps in Figure 5. The placement of the isotherms may be compared with Figure 3. Any heat transfer modelling involving the possibility of defected fuel melting (oxidizing conditions) must be consistent with this figure to capture the combine effects of thermal energy transfer and related phase changes.

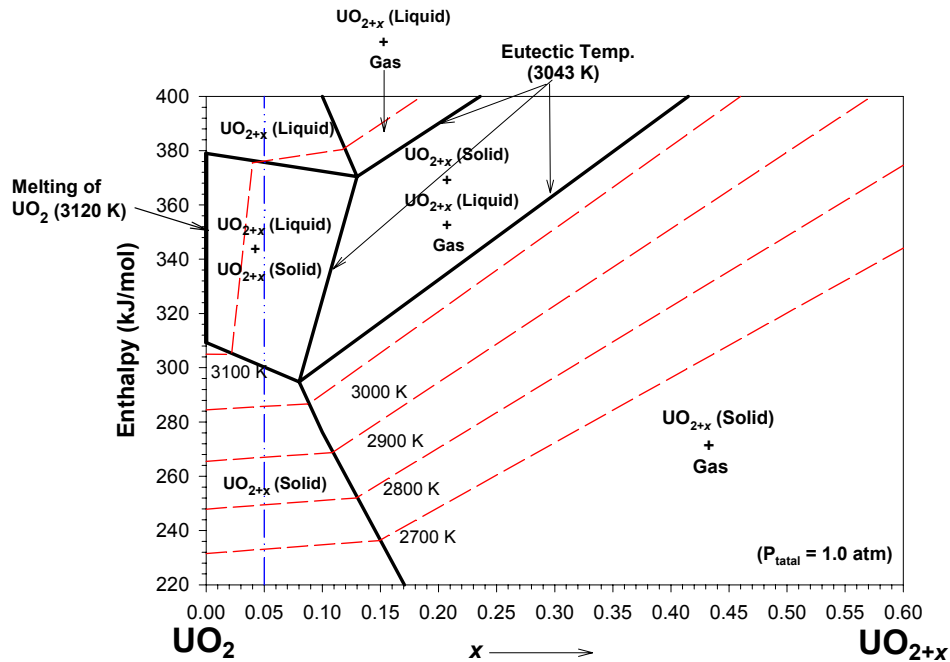


Figure 6: Enthalpy-composition phase diagram in the vicinity of the melting of UO_{2+x} .

(iii) *Inclusion of fission products (ZrO_2)*

Inclusion of fission products in fuel adds a further complication in dealing with the possibility of melting. Consider as an example ZrO_2 in UO_2 . A thermodynamic treatment of the phase diagram was published recently⁽⁸⁾. In the present work, emphasis was placed on the solubility of ZrO_2 at the eutectoid temperature. The Gibbs energy isotherms in Figure 7 yield mole fractions of UO_2 in the tetragonal and cubic solid solutions of 0.028 and 0.996, respectively. Figure 8 shows the complete computed phase diagram for this system in comparison with experimental data.⁽⁹⁻¹³⁾

The model for the U-O binary system may be combined with the treatment for the UO_2 - ZrO_2 system by interpolation (Toop⁽¹⁴⁾-Kohler⁽¹⁵⁾) to generate the possible phase appearances in the UO_2 - UO_3 - ZrO_2 system. Again, it is emphasized that the mole fraction of UO_3 in this system is a formal way of representing the non-stoichiometry in UO_{2+x} solid or liquid phase. A provisional phase diagram at 3000 K is shown in Figure 9. Of note is the suppression of the melting temperature of UO_2 and the tendency of ZrO_2 to concentrate in the liquid phase. Models of fuel melting therefore must not only deal with a potentially moving interface but also with multicomponent mass transfer considerations.

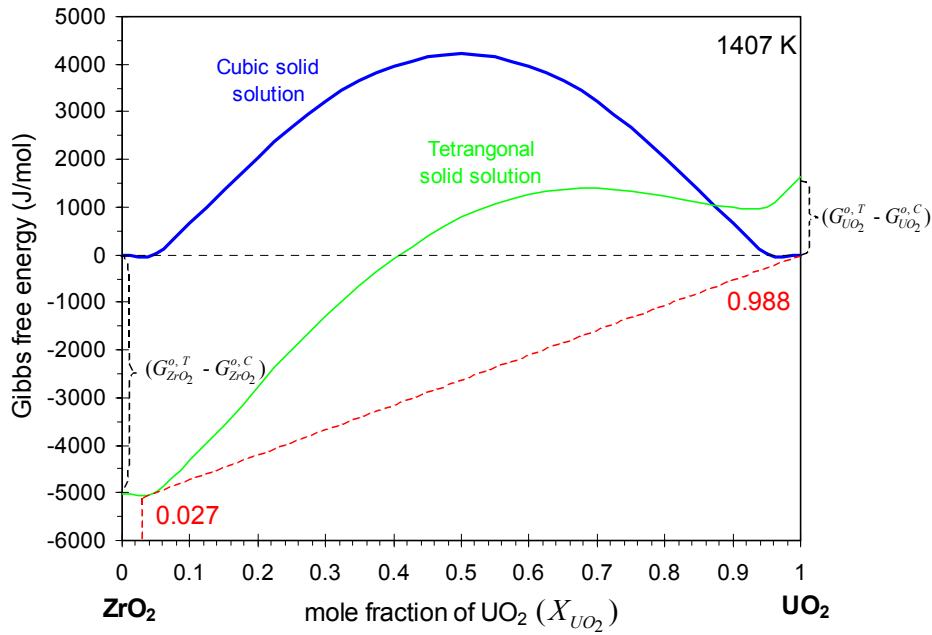


Figure 7: Gibbs free energy isotherms at eutectoid temperature (1407 K) for cubic and tetragonal solid solutions for ZrO_2 - UO_2 system.

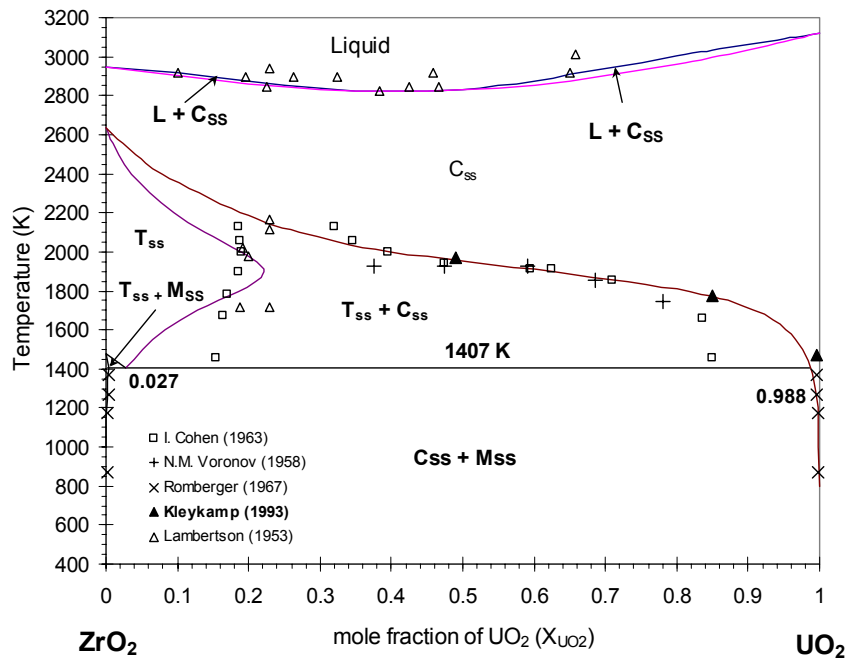


Figure 8: Computed ZrO_2 - UO_2 binary system along with experimental data. (Mss = monoclinic, Tcc = Tetragonal and Css = cubic solid solutions)

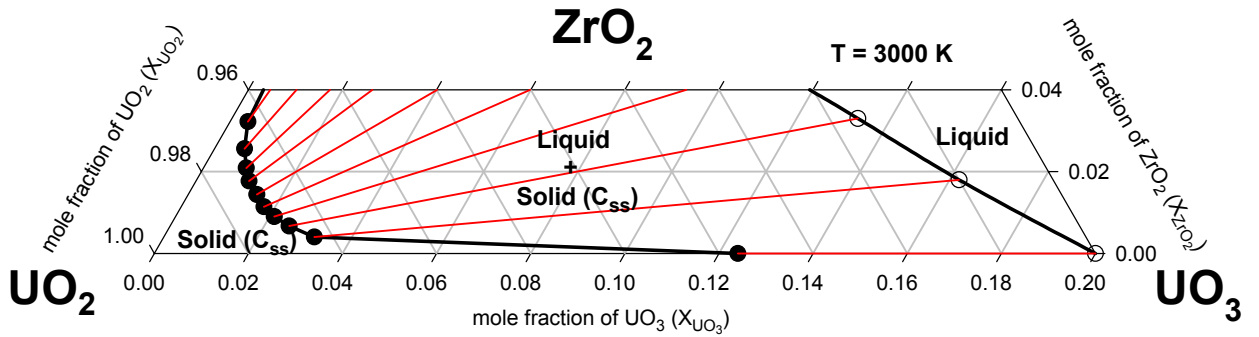


Figure 9: Computed provisional ternary phase diagram for $\text{UO}_2\text{-UO}_3\text{-ZrO}_2$ system at 3000 K.

2.0. HEAT AND MASS TRANSFER MODEL DEVELOPMENT

A treatment is needed to describe the melting behaviour of fuel to better determine operational limits with defected fuel as well as for the risk prediction of potential severe reactor accidents. For an accurate temperature prediction, one requires a combined mathematical model for both the oxygen mass transport and heat conduction for fuel containing a molten core (see Figure 10).

Diffusion of oxygen in both the liquid and solid is assumed to be governed by the Fick's second law⁽¹⁶⁾ :

$$\frac{\partial c(\vec{r}, t)}{\partial t} = \vec{\nabla} \cdot [D(c(\vec{r}, t)) \vec{\nabla} c(\vec{r}, t)] + R(\vec{r}, t) \quad (3)$$

where the concentration of oxygen $c(\vec{r}, t)$ is a function of both position (\vec{r}) and time (t) and $R(\vec{r}, t)$ is the mass source term. $D(c(\vec{r}, t))$ is the diffusion coefficient of the solute in either the liquid or solid phase of the hyperstoichiometric fuel, which depends on both temperature and concentration. This problem is better known as a Stefan problem since the solid and liquid phases will change size over time that introduces a moving-boundary condition. It is implicitly assumed that there is no bulk convection in the liquid core.

Analogously, the corresponding equation describing the heat conduction is given by⁽¹⁶⁾ :

$$\rho C_p \frac{\partial T(\vec{r}, t)}{\partial t} = \vec{\nabla} \cdot [k(T(\vec{r}, t)) \vec{\nabla} T(\vec{r}, t)] + Q(\vec{r}, t) \quad (4)$$

where $T(\vec{r}, t)$ is the temperature, ρ is the fuel density, C_p is the specific heat, k is the thermal conductivity and $Q(\vec{r}, t)$ is the heat source term.

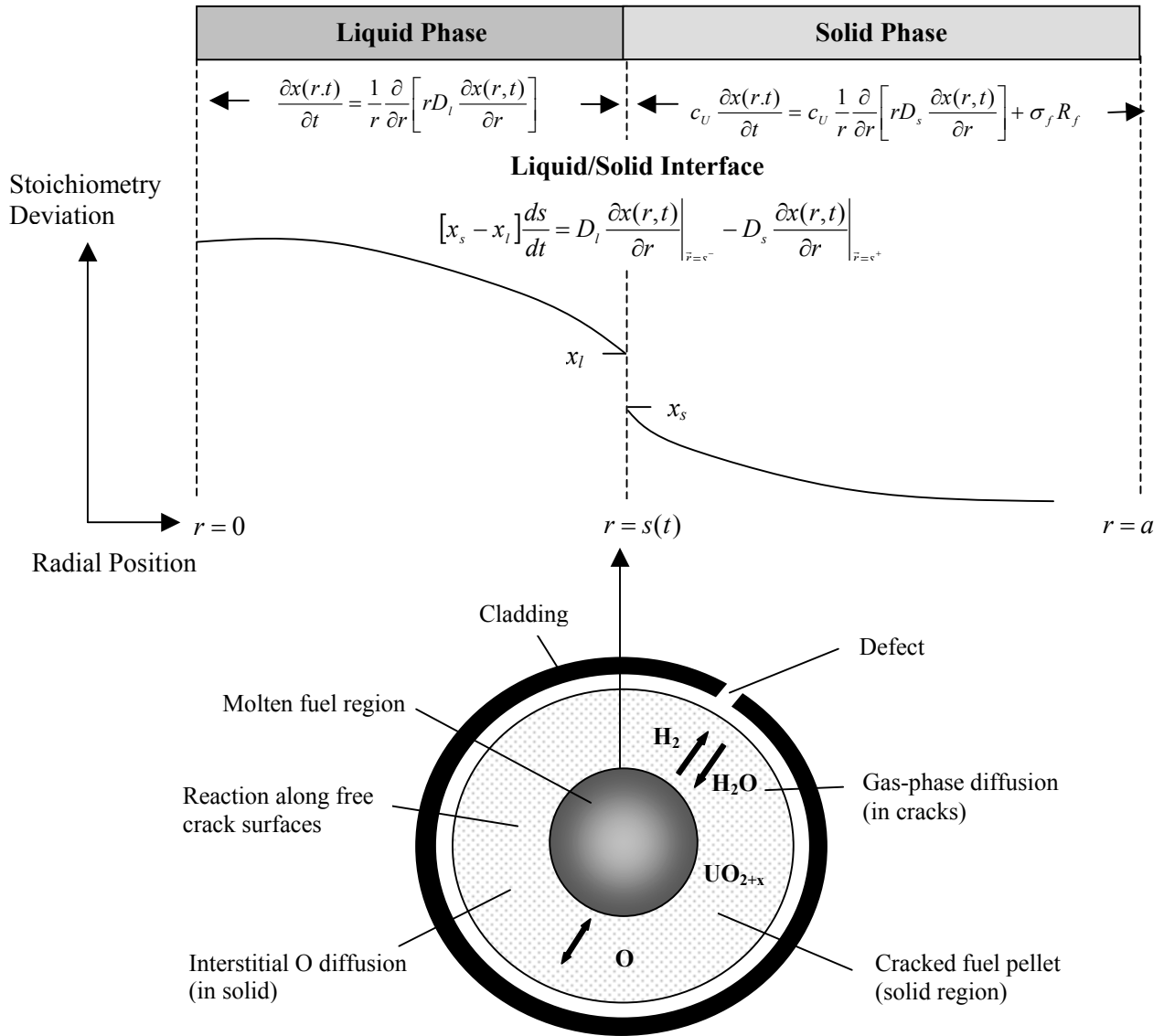


Figure 10: Schematic diagram showing the radial profile for the stoichiometry deviation in a fuel pellet across a liquid/solid interface at a particular time t (upper figure) and a radial cross-section of the fuel pellet showing a molten and solid region (lower figure).

As shown in Figure 10, the variable $s(t)$ describes the position of the liquid (l)/solid (s) interface that varies with time. For fuel oxidation kinetics modeling, the Stefan problem can be stated more fully for the simple radial diffusion of oxygen in a cylindrical fuel pellet of radius a as:^(5, 16, 17)

$$\frac{\partial x}{\partial t} = \frac{1}{r} \frac{\partial}{\partial r} \left[r D_l \frac{\partial x}{\partial r} \right], \quad 0 < r < s(t) \quad (5a)$$

$$c_U \frac{\partial x}{\partial t} = c_U \frac{1}{r} \frac{\partial}{\partial r} \left[r D_s \frac{\partial x}{\partial r} \right] + \sigma_f R_f, \quad s(t) < r < a \quad (5b)$$

$$J_s - J_l = - \left(D_s \frac{\partial x}{\partial r} \Big|_{r=s(t)^+} - D_l \frac{\partial x}{\partial r} \Big|_{r=s(t)^-} \right) = [x_s - x_l] \frac{ds}{dt}, \quad r = s(t) \quad (5c)$$

Here x is the stoichiometry deviation in UO_{2+x} , c_U (mol m^{-3}) is the molar density of uranium, σ_f is the surface area of cracks per unit volume of fuel (m^{-1}) for the cracked (solid) fuel body and R_f is the rate of reaction for either fuel oxidation or reduction due to steam migration into the cracks of the solid portion of the pellet as detailed in Ref. (16). The first equation describes oxygen diffusion in the liquid phase (l) to the left of the interface in Figure 10. The second equation refers to oxygen diffusion in the solid phase (s) to the right of the interface in Figure 10. The effect of thermodiffusion (i.e., the Soret effect) has not been considered in this analysis⁽¹⁶⁾. The third equation is a differential equation for the velocity of the melting front (ds/dt). It describes the moving boundary condition at the liquid/solid interface with a conservation of flux J , where there is a discontinuity in the solute (oxygen) concentration at the interface. There is no source of oxygen in Eq. (5a) since steam-filled cracks cannot penetrate into the liquid zone (instead oxygen is supplied via the boundary condition in Eq. (5c)). This concentration discontinuity for x_l and x_s in Figure 10 can be determined from experiments or from the U-O phase diagram with the placement of the solidus and liquidus lines (at a given temperature T) (see Figure 1)^(1-3,5). A Neumann/reflexive condition, $\partial x/\partial r = 0$, can be used at the pellet centreline to account for the symmetry ($r = 0$) and at the pellet surface ($r = a$) (assuming no loss of oxygen).

Similarly, for heat conduction, the analogous relations are:^(16, 18)

$$(\rho C_p)_l \frac{\partial T}{\partial t} = \frac{1}{r} \frac{\partial}{\partial r} \left[r k_l \frac{\partial T}{\partial r} \right] + \frac{P}{\pi a_p^2}, \quad 0 < r < s(t) \quad (6a)$$

$$(\rho C_p)_s \frac{\partial T}{\partial t} = \frac{1}{r} \frac{\partial}{\partial r} \left[r k_s \frac{\partial T}{\partial r} \right] + \frac{P}{\pi a_p^2}, \quad s(t) < r < a \quad (6b)$$

$$J_s - J_l = - \left(k_s \frac{\partial T}{\partial r} \Big|_{r=s(t)^+} - k_l \frac{\partial T}{\partial r} \Big|_{r=s(t)^-} \right) = \rho L \frac{ds}{dt}, \quad r = s(t) \quad (6c)$$

where C_p ($\text{kJ kg}^{-1} \text{K}^{-1}$) is the specific heat, k ($\text{kW m}^{-1} \text{K}^{-1}$) is the thermal conductivity, P is the fuel element linear rating (kW m^{-1}) and L is the latent heat of melting or solidification. It is implicitly assumed in Eq. (6c) that the density does not change during the melting or solidification process (i.e., the density can be reasonably approximated as $\rho \sim (\rho_s + \rho_l)/2$ at the liquid/solid interface for the current problem). The effect of flux depression has not been considered in this analysis.

Instead of tracking the motion of the moving boundary across a fixed grid, a transformation can be imposed which fixes the interface instead^(17, 19). Thus, defining the two

new positional variables $u(t) = \frac{r}{s(t)}$ and $v(t) = \frac{r-s(t)}{a-s(t)}$, the interval $0 < r < s(t)$ now coincides

with $0 < u < 1$ while the interval $s(t) < r < a$ coincides with $0 < v < 1$. Writing $x_p(u, t)$ as the stoichiometry deviation in the liquid phase (which corresponds to $x(r, t)$ in $0 < r < s(t)$) and $x_q(v, t)$ in

the solid phase (corresponding to $x(r,t)$ in $s(t) < r < a$). Hence, for these variable transformations, Eq. (5) becomes:⁽¹⁷⁾

$$s(t)^2 \frac{\partial x_p(u,t)}{\partial t} - us(t) \frac{\partial x_p(u,t)}{\partial u} = \frac{1}{r} \frac{\partial}{\partial u} \left[r D_l(x_p(u,t)) \frac{\partial x_p(u,t)}{\partial u} \right], \quad 0 < u < 1 \quad (7a)$$

$$[a - s(t)]^2 c_v \frac{\partial x_q(v,t)}{\partial t} - (1-v)[a - s(t)] \frac{ds}{dt} \frac{\partial x_q(v,t)}{\partial v} = c_u \frac{1}{r} \frac{\partial}{\partial v} \left[r D_s(x_q(v,t)) \frac{\partial x_q(v,t)}{\partial v} \right] + [a - s(t)]^2 \sigma_f R_f, \quad 0 < v < 1 \quad (7b)$$

$$\left(\frac{D_l(x_p(u,t)) \frac{\partial x_p(u,t)}{\partial u} \Big|_{u=1}}{s(t)} - \frac{D_s(x_q(v,t)) \frac{\partial x_q(v,t)}{\partial v} \Big|_{v=0}}{a - s(t)} \right) = [x_s - x_l] \frac{ds}{dt}, \quad u = 1; \quad v = 0 \quad (7c)$$

Similarly, writing $T_p(u,t)$ as the temperature in the liquid phase (which corresponds to $T(r,t)$ in $0 < r < s(t)$) and $T_q(v,t)$ in the solid phase (corresponding to $T(r,t)$ in $s(t) < r < a$), Eq. (6) becomes:

$$s(t)^2 (\rho C_p)_l \frac{\partial T_p(u,t)}{\partial t} - us(t) \frac{\partial T_p(u,t)}{\partial u} = \frac{1}{r} \frac{\partial}{\partial u} \left[r k_l(T_p(u,t)) \frac{\partial T_p(u,t)}{\partial u} \right] + s(t)^2 \left(\frac{P}{\pi a^2} \right), \quad 0 < u < 1 \quad (8a)$$

$$[a - s(t)]^2 (\rho C_p)_s \frac{\partial T_q(v,t)}{\partial t} - (1-v)[a - s(t)] \frac{ds}{dt} \frac{\partial T_q(v,t)}{\partial v} = \frac{1}{r} \frac{\partial}{\partial v} \left[r k_s(T_q(v,t)) \frac{\partial T_q(v,t)}{\partial v} \right] + [a - s(t)]^2 \left(\frac{P}{\pi a^2} \right), \quad 0 < v < 1 \quad (8b)$$

$$\left(\frac{k_l(T_p(u,t)) \frac{\partial T_p(u,t)}{\partial u} \Big|_{u=1}}{s(t)} - \frac{k_s(T_q(v,t)) \frac{\partial T_q(v,t)}{\partial v} \Big|_{v=0}}{a - s(t)} \right) = \rho L \frac{ds}{dt}, \quad u = 1; \quad v = 0 \quad (8c)$$

For a solution of the coupled partial differential equations in Eqs. (7) and (8), the material properties of ρ , C_p , k for liquid and solid hyperstoichiometric uranium dioxide need to be determined. In addition, the oxygen diffusion coefficients for the liquid and solid phase of the fuel are required.

The heat capacity, thermal conductivity and density for the solid hyperstoichiometric fuel can be taken from Ref. (16). The latent heat of solidification (or enthalpy of fusion) can be taken from that for UO_2 , i.e., $L \sim 70 \text{ kJ mol}^{-1}$.⁽⁶⁾ For liquid fuel, correlations for ρ_l (Mg m^{-3}), $(C_p)_l$ ($\text{J mol}^{-1} \text{K}^{-1}$), k_l ($\text{W m}^{-1} \text{K}^{-1}$) as a function of temperature T (K) for uranium dioxide can also be used where:⁽⁶⁾

$$\rho_l = 8.860 - 9.285 \times 10^{-4} (T - 3120), \quad 3120 \leq T \leq 4500 \quad (9a)$$

$$(C_p)_l = 0.25136 + \frac{1.3288 \times 10^9}{T^2} \quad (9b)$$

$$k_l = 2.5 \quad (9c)$$

The diffusion coefficient for oxygen diffusion in hyperstoichiometric solid fuel as a function of temperature T (K) is given by:⁽²⁰⁾

$$D_s = 2.5 \exp\left(-\frac{16400}{T}\right) \text{ cm}^2 \text{ s}^{-1} \quad (10)$$

For the diffusion of solute A (oxygen) in solvent B (liquid UO_2), the classical Stokes-Einstein equation can be employed:⁽²¹⁻²³⁾

$$D_l = D_{AB} = \frac{k_B T}{6\pi r_A \eta_B} \text{ cm}^2 \text{ s}^{-1} \quad (11)$$

where k_B is Boltzmann's constant ($= 1.381 \times 10^{-23}$ J/K), η_B is the viscosity of molten $\text{UO}_2 = 0.988 \times 10^{-3} \exp\{4620/T(\text{K})\}$ Pa s,⁽⁶⁾ and r_A is the radius of the "spherical" solute (which can be estimated as the Van der Waal's radius for oxygen $= 1.4 \times 10^{-10}$ m)⁽²⁴⁾.

As currently underway, the coupled equations can be solved using a finite element technique with the commercial FEMLAB platform.

3.0 CONCLUSIONS

Modelling physiochemical phenomena associated with fuel oxidation involves a coupling of boundary conditions in a multicomponent system governed by chemical thermodynamics with interrelated differential equations dealing with both heat and mass transfer considerations. Since the onset of centerline melting is an upper-boundary operating condition with a defected element, the authors are attempting to advance a first-principles fuel oxidation model that includes the molten fuel domain. This paper highlights the very considerable complications that arise when the fuel may possibly start to melt.

4.0 ACKNOWLEDGEMENTS

The authors would like to acknowledge funding provided by the Natural Science and Engineering Research Council of Canada (NSERC) and the Director General of Nuclear Safety.

REFERENCES

1. B.J. Lewis, W.T. Thompson, F. Akbari, D.M. Thompson, C. Thurgood and J. Higgs, "Thermodynamic and Kinetic Modelling of the Fuel Oxidation Behaviour in Operating Defective Fuel", *J. Nucl. Mater.* 328 (2004) 180-196.
2. P.-Y. Chevalier, E. Fischer and B. Cheynet, "Progress in the Thermodynamic Modelling of the U-O Binary System", *J. Nucl. Mater.* 303 (2002) 1.
3. C. Guéneau, M. Baichi, D. Labroche, C. Chatillon and B. Sundman, "Thermodynamic Assessment of the Uranium-Oxygen System", *J. Nucl. Mater.* 304 (2002) 161.
4. R.E. Latta, and R.E. Fryxell, "Determination of Solidus-Liquidus Temperatures in the UO_{2+x} System ($-0.50 < x < 0.20$)", *J. Nucl. Mater.* Vol.35, No. 2 (1970) 195.
5. D. Manara, C. Ronchi, M. Sheindlin, M. Lewis and M. Brykin, "Melting of Stoichiometric and Hyperstoichiometric Uranium Dioxide", *J. Nucl. Mater.* 342 (2005) 148-163.
6. J.K. Fink, "Thermophysical Properties of Uranium Dioxide", *J. Nucl. Mater.* 279 (2000) 1-18.
7. L.V. Matweev and M.S. Veshchunov, "Modelling of High Temperature Superionic Transition of Uranium Dioxide Crystals", *J. Nucl. Mater.* Vol. 265 (1999) 285-294.
8. M. Yashima, T. Koura, Y. Du and M. Yoshimura, "Thermodynamic Assessment of the Zirconia-Urania System", *Journal of American Ceramic Society*, Vol. 79, No. 2 (1996) 521-524.
9. I. Cohen and B.E. Schaner, "A Metallographic and X-ray Study of the UO_2 - ZrO_2 System", *Journal of Nuclear Materials*, Vol. 9, No. 1 (1963) 18-52.
10. N.M. Vorovov, E. A. Voitekhova and A.S. Danilin, "Phased Equilibrium of the UO_2 - ZrO_2 System", *Proceedings of the 2nd U.N. International Conference on Peaceful Uses of Atomic Energy*, United nations, New York, Vol. 6 (1958) 221-225.
11. K.A. Rogmerger, C.F. Bases, Jr., and H.H. Stone, "Phase Equilibrium Studies in the UO_2 - ZrO_2 System", *Journal of Inorganic Nuclear Chemistry*, Vol. 29, No. 7 (1967) 619-630.
12. H. Kleykamp, "The Solubility of Selected Fission Products in O_2 and $(U,Pu)O_2$ ", *J. Nucl. Mater.*, Vol. 206 (1993) 82-86.
13. W.A. Lambertson and M.H. Mueller, "Uranium Oxide Phase Equilibrium Systems III. UO_2 - ZrO_2 ", *Journal of American Ceramic Society*, Vol. 36, No. 11 (1953) 365-368.
14. G.W. Toop, *Trans. Met. Soc. AIME*, Vol. 233 (1965) 850.
15. F. Kohler, *Montas. Chem.*, Vol. 91 (1960) 738-740.

16. J.D. Higgs, B.J. Lewis W.T. Thompson and Z. He, "Modelling of Fuel Oxidation Behaviour for Defected Fuel", *9th International Conference on CANDU Fuel*, Belleville, Ontario, September 18-25 (2005).
17. T.C. Illinworth, I.O. Golosnoy, Y.V. Gergely and T.W. Clyne, "Numerical Modelling of Transient Liquid Phase Bonding and Other Diffusion Controlled Phase Changes", *J. Mat. Sci.* v. 40, no. 9-10 (2005) 2505-2511.
18. S. Kakac and Y. Yener, "Heat Conduction", second edition, Hemisphere Publishing Corporation, New York, (1985).
19. J. Crank, "The Mathematics of Diffusion," Oxford, UK (1984).
20. J.A. Meachen, "Oxygen Diffusion in Uranium Dioxide", *Nuclear Energy*, Vol. 28, No. 4, (1989) 221-226.
21. R.C. Reid, J.M. Prausnitz and B.E. Poling, "The Properties of Gases and Liquids", McGraw-Hill Book Company, New York, (1987).
22. J. Rest and A.W. Cronenberg, "Modeling the Behavior of Xe, I, Cs, Te, Ba, and Sr in Solid and Liquefied Fuel during Severe Accidents", *J. Nucl. Mater.* 150 (1987) 203-225.
23. B.J. Lewis, B. Andre, B. Morel, P. Dehaut, D. Maro, P.L. Purdy, D.S. Cox, F.C. Iglesias, M.F. Osborne and R.A. Lorenz, "Modelling the Release Behaviour of Cesium During Severe Fuel Degradation", *J. Nucl. Mater.* 227 (1995) 83-109.
24. "Handbook of Chemistry and Physics", CRC Press, Cleveland, Ohio (1975) D-178.